ANNEXE A.1.2 Bilan d'erreur sur l'étalonnage absolu du capteur SPOT-HRV sur les sites tests de White Sands et La Crau

Uncertainties in the calibration of SPOT sensors with reference to test-sites White Sands and La Crau

R. Santer, C. Schmechtig, K. Thome

Soumis à Remote Sensing of the Environment.

Uncertainties in the calibration of SPOT sensors with reference to test-sites White Sands and La Crau

R. Santer*, C. Schmechtig*, K. Thome**
*Université du Littoral, station marine de Wimereux
BP80 62930 Wimereux FRANCE
**Remote Sensing Group, Optical Sciences Center,
University of Arizona P.O Box 210094, Tucson, Az

INTRODUCTION

The vicarious calibration of SPOT-1 HRV at White Sands began in 1985 and since then, 31 calibration days have been collected. For La Crau, the first calibration occurred in 1989 and data have been collected on 27 days. All of these data have been published mostly as internal reports. We first want to reprocess the data for several reasons. First, because some assumptions have changed over time. For example, the imaginary part of the index of refraction for aerosols at White Sands has changed from the original value of 0.01 to 0.005. There have also been changes in the methods for describing gaseous absorption. First, the water vapor absorption which mainly affects the XS3 band was computed using a water vapor optical thickness but this is problematic since water vapor absorption is not exponential. The 5S code, used since 1987 and recently upgraded to the 6S code included the water vapor continuum and certainly a better estimate of the transmittance because the spectral resolution was improved. The same improvements were brought to the scattering part of the radiative transfer codes. Because of improvements in computers, it is now possible to calculate the radiative transfer at much higher angular resolution and larger number of layers for discretizing the optical thickness. It is now also possible to have more physical codes including such effects as polarization which leads to some impact on the radiance 1evels for XS1. Even if the calibration procedures between the two groups at the University of Arizona and the University of Lille have been compared during a campaign in April 1993 (Chami et al., 1994), and the results agree within a few percent, for consistency, it was better to reprocess the data using the same protocols.

In a companion paper (Schmechtig et al., this issue), we developed BRDF models for the two sites and compared the results of predicted calibration.

Reprocessing all of the calibration days was also a good opportunity to introduce error bars and have a robust budget analysis while only limited indications on the accuracy have been given in the past (Santer et al., 1992, Biggar et al., 1994). Through this error analysis we want to see.

ERROR BUDGET

Error calculation

For each 31 calibration data sets for White Sands and the 27 sets of data from La Crau, we evaluate the uncertainties using the 6S code. The calibration coefficient far the k^{th} bands of HRV
(four bands total – XS1, XS2, XS3, and PAN) can be given as

$$A_k = \frac{DN_k \mu_s \pi}{G_{(m,k)} \rho_k E_k} \qquad \textbf{(1)}$$

where ρ_k is the apparent reflectance at the top of the atmosphere for the k^{th} band as determined by radiative transfer code calculations based on measurements made at the site at the time of sensor overpass, μ_s is the cosine of the solar zenithal angle, $G_{(m,k)}$ is the m^{th} system gain for the k^{th} band, DN_k are the digital numbers of the test site reported for the k^{th} band, and E_k is the solar constant averaged over the k^{th} band corrected for earth-sun distance. To estimate overall uncertainty, we differentiate (1) and root sum square the component uncertainties. This implicitly assumes that the errors are random and independent, which is not necessarily the case, but this approach, while simplistic is still sufficient to allow us to determine the importance of the various uncertainty sources. Thus, the error in the calibration coefficient can be written as

$$\frac{\Delta A_k}{A_k} = \sqrt{\left(\frac{\Delta \rho_k}{\rho_k}\right)^2 + \left(\frac{\Delta \mu_s}{\mu_s}\right)^2 + \left(\frac{\Delta DN_k}{DN_k}\right)^2 + \left(\frac{\Delta E_k}{E_k}\right)^2} \qquad \textbf{(2)}$$

While it is possible to obtain results relative to the solar constant, E_k, we include the solar constant here for reference. Further discussion will omit this term as many groups operate in terms of reflectance, or other relative units, thus avoiding uncertainties due to this factor. However, it should be kept in mind that when the reflectance-based results are taken to absolute radiometric units, that this solar uncertainty is present.

Apparent reflectance

The 6S code is used here for the radiative transfer calculations. While there are accuracy limitations to this code, the computational efficiency of the code and its ability to produce band- averaged results makes it a good choice to examine multiple cases. The problem is treated as a sensitivity study and thus a single standard run of the radiative transfer code is used for reference. We then vary one of the input parameters to determine the change in the apparent reflectance due to this change in the parameter. The parameters that were varied in this work are solar zenith angle, atmospheric pressure, sensor spectral response, water vapor content, ozone content, aerosol parameters (real and imaginary index and spectral optical depth), surface reflectance (BRDF effects and surface inhomogeneity)

The estimated uncertainty in the solar zenith angle is ±0.2 degrees. This is primarily due to uncertainties in the time of sensor overpass. This uncertainty leads to an uncertainty in the apparent reflectance that is at a maximum around the winter solstice due to the lower solar zenith. For typical zenith angles at both sites at this time of year, the largest uncertainty in apparent reflectance due to solar zenith angle uncertainty is 0.5%.

The uncertainty in digital numbers is due to instrumental noise and site inhomogeneities. The site inhomogeneities dominates this uncertainty and leads to uncertainties in the average digital numbers due to misregistration between the site in the image and the site that is characterized on the ground. This inhomogeneity effect does not include atmospheric adjacency issues but instead only refers to errors in registration. Assuming that the site can be located to within a single pixel using large tarpaulins on the ground as ground-control points, studies of past surface reflectance measurements and examination of old imagery, we estimate that the error made on the evaluation of the digital counts is ±0.5. For the bands of HRV, this leads to approximately an 0,3% uncertainty in the predicted digital numbers of the site.

Atmospheric pressure is used to determine the molecular scattering optical thickness. Uncertainty in this parameter has two effects. The first is straightforward and it is the effect on the value of the molecular optical thickness and this leads to an incorrect assessment of molecular scattering. The second effect is that the molecular optical thickness is subtracted from the total optical thickness to help determine aerosol properties. Only the first type of uncertainty is considered here. The elevation of White Sands is 1196 m. This leads to a mean pressure of 880 hPa with a range of typical values from 870 hPa to 890 hPa. At La Crau, the elevation is 20 m and the pressure typically varies between 1000 hPa and 1013 hPa. This leads to uncertainties in the predicted apparent reflectance of less than 0.3%.

The retrieval of columnar water vapor should be to better than 10% at values of 1.0 cm or greater and a value of 10 mm at lower water vapor amounts [Thome et al., 1993]. To study the effect of water vapor uncertainty, we assumed an uncertainty of 20%. Figure 1 shows the results of the change in apparent reflectance for the 58 total cases at White Sands and La Crau. These results are for the XS3 band (850nm) which has the highest sensitivity to water vapor and are shown in terms of the slant path water vapor amount for the solar zenith angle. As can be seen from the figure, the uncertainty at White Sands is less than 0.5%, mostly due to the fact that there is typically less water vapor at this site than at La Crau. The value at La Crau is still less than 1.1% in the worst case for this overestimated uncertainty in columnar water vapor.

For columnar ozone, we assume an uncertainty of ±10%. The effect of columnar ozone uncertainty is most important in the channels XS1 and XS2. (550nm and 650nm) but will vary for each of the HRV cameras on the different SPOT platforms due to small changes in the spectral response from one sensor to the next. Table 1 summarizes the percent change in apparent reflectance due to estimated uncertainties in the columnar ozone. The values are shown for both SPOT-2 and SPOT-3 HRV. Since ozone amount will vary depending upon the day of year and latitude of the site, the results are shown for several times of the year for both sites corresponding to time periods for which calibrations are performed.

Spectral responses

The HRV spectral responses are characterized on the ground prior to launch. An identical set of witness filters were installed in a vacuum chamber and where their spectral responses were monitored. From these measurements, it appears that there could possibly be a shift of the XS2 band's cutoff response by as much as 10 nm. That is, the filter widened by 10 nm on the red side of the bandpass. These data imply that we should also account for uncertainties in the spectra1 response. For this study, we investigate the uncertainty due to spectral response by translating the response of each band by ±5nm.

Aerosols

For simplicity in this study, we treat the aerosol size distribution to be described by a power law, or Junge distribution. Thus, there are four different parameters that are used to fully describe the aerosols in the radiative transfer: the extinction optical depth, the Junge parameter, and the real and imaginary indexes of refraction.

To estimate the error due to uncertainty in the extinction optical depth, it helps to first understand how this parameter is determined. The standard method relies on applying Beer's Law to ground-based solar radiometer measurements of the spectral solar irradiance:

$$E(\lambda) = \mu_s E_s(\lambda) e^{-m\delta} \quad \textbf{(3)}$$

where $E(\lambda)$ is the measured irradiance at the surface at wavelength λ, E_s, is the solar irradiance incident at the top of the earth's atmosphere in the bands of the solar radiometer, m is the optical airmass, and δ is the total extinction optical depth. The extinction optical thickness can be written as the sum of the molecular, ozone, and aerosol optical thicknesses.

From this, it can be shown that

$$\Delta\delta_{aerosol} = \sqrt{(\Delta\delta_{molec})^2 + (\Delta\delta_{O3})^2 + \left(\frac{\mu_s \Delta E_s}{E_s}\right)^2} \quad \textbf{(4)}$$

Where $\Delta\delta_{aerosol}$ is the uncertainty in the aerosol extinction optical depth, $\Delta\delta_{molec}$ is the uncertainty in the molecular optical thickness, and $\Delta\delta_{O3}$, is the uncertainty in the estimate of the relative ozone absorption optical depth. Based on extensive experience with the solar radiometers used in our work, we have found that the uncertainties in the molecular optical thickness (due primarily to uncertainty in measured atmospheric pressure) and that due to ozone are much smaller than that due to the third term which is related to the system calibration. With careful measurements at high-altitude sites, it is possible to keep the uncertainty in the sensor calibration to less than 1% [Gellman et al., 1991]. In some cases, it is not possible to have such a careful calibration, thus for this work we use an overestimate of this uncertainty and assume the radiometer's calibration to be have an uncertainty of 2%. This 2% uncertainty leads to $\Delta\delta_a$=0.02 for typical sun angles and atmospheric conditions at the two sites.

This uncertainty is assumed to be the same for both sites. The uncertainty due to the other three parameters, size distribution and indexes of refraction, on the other hand are treated separately for each site.

At White Sands, the calibration work for HRV assumes a Junge distribution to describe the size distribution (Biggar et al., 1993). The aerosols are assumed to have a real index of refraction of 1.44 and an imaginary index of 0.005. For the purposes of this study, we restricted the size of the aerosols such that the radii are between 0.02 and 5.02 μm. We allowed the real index to vary from 1.40 to 1.55 and the imaginary index to have values from 0.001 to 0.015. The Junge parameter is assumed to have an uncertainty of 0.2 and the aerosol extinction optical depth is known to 0.01 that corresponds to the 5% uncertainty from previous work (Biggar et al., 1993).

Assuming that the errors due to these factors can be treated as root-squared sum, we have determined the uncertainty in the apparent reflectance due to uncertainties in the aerosol parameterization. The results of this are shown in Figure 2 as a function of optical depth for the 31 cases at White Sands. Also shown in the figure are the uncertainties due solely to that of the imaginary index of refraction. As can be seen from the figure, it is clear that the uncertainty in this parameter dominates the overall uncertainty of the problem. This is to be expected at a

high-reflectance site such as White Sands, where the reflected solar beam dominates the signal at the top of the atmosphere.

La Crau is treated differently than White Sands because more detailed measurements of the aerosol's radiative properties are made at this site. For the La Crau data, we assumed uncertainties in the extinction optical depth of 0.005 and 0.02 based on past studies at the site [Devaux et al]. For the Junge parameter we assumed a somewhat smaller uncertainty of 0.1 because the La Crau data sets include sky radiance measurements in the size distribution retrieval. The real index was assumed to cover the same range of values as at White Sands (1.40 to 1.55) and the range of radii used is 0.01 to 10.0 μm. Based on these values, and knowledge of the molecular optical thickness, we can determine the error budget for the single scattering albedo [Devaux et al]

$$\frac{\Delta \omega_0}{\omega_0} = \sqrt{\left(\frac{\Delta \delta^a_{ext}}{\delta^a_{ext}} \right)^2 + \left(\frac{\Delta C}{C} \right)^2 + \left(1 + \frac{\delta^m}{\delta^a_{sca}} \right)^2} \qquad \textbf{(5)}$$

Where ω_o is the single scattering albedo defined as $\delta^a_{sca}/\delta^a_{ext}$, δ^a_{ext} is the total extinction optical depth due to aerosols, δ^m is the molecular scattering optical depth, and δ^a_{sca} is the optical thickness due to scattering by aerosols. The value used for $\Delta C/C$ is 5%. From the value for the uncertainty in the single scattering albedo derived in (5), it is possible to estimate the uncertainty in the imaginary index.

Figure 3 shows the uncertainty in top-of-the-atmosphere reflectance due to aerosol uncertainties at the La Crau site. The figure shows four values of uncertainties related to the uncertainties due to all factors combined for the two optical thickness uncertainties (the global values) and the uncertainty due solely to imaginary index uncertainty for each of the optical thickness cases. The first thing to note is the difference in the scale of the x-axis between Figures 2 and 3. The results in both figures 2 and 3 are very similar in magnitude and show similar dominance of the imaginary index in the uncertainties. From this, it should be clear why aerosol uncertainties are more important at La Crau then for White Sands. The figure also shows that the uncertainty due to aerosols is greater for an extinction optical depth error of 0.02 than for 0.005. It also appears that the uncertainty in reflectance due aerosol uncertainties decreases for optical thicknesses greater than about 0.40. It is not clear at this time what causes this to occur.

BRDF effects

The BRDF effects of the surface on the calibration is discussed in detail in an accompanying paper in this issue (Schmechtig et al.). Experimental data were fit with polynomials to remove surface heterogeneity from the measurements. The experimental data consisted of collecting directional radiances in the principal plane and in a perpendicular plane to it, and fit with a Fourier series expansion. The Fourier series expansion of the reflectance is directly suitable for use with the successive orders of scattering radiative transfer code. Determination of the BRDF includes removal of the diffuse component of the downwelling irradiance from the measurements with an iterative approach. The bias is of the order of several percent for both sites and varies from campaign to campaign due to changing solar and view conditions.

Environment effects

The term adjacency effect, or also environment effect, is used to describe the effect that the area surrounding the target has on the radiance measured from the target. That is, the radiance measured from a dark target surrounded by a bright area (lake surrounded by snow-covered land) will be different than that from the same dark target surrounded by an area which is not bright (lake surrounded by land composed of dark soil). This effect is a function of the target size, the reflectance of the target and surround, and the amount of atmospheric scattering.

Estimates of this effect are typically made using Monte Carlo simulation models that can account for any type of scene. However, Monte Carlo simulations are time consuming, so we have used the formulation for adjacency effects from the 5S radiative transfer code

$$\rho = \rho_{atm} + \frac{T(\mu_s)}{1 - <\rho>}\left(\rho_T e^{-\delta/\mu_v} + <\rho> t_d(\mu_v)\right) \quad \textbf{(6)}$$

where ρ_{atm} is the reflectance due to the atmosphere alone, ρ_T is the surface reflectance of the target of interest, $<\rho>$ is the average background reflectance, $T(\mu_s)$ is the transmittance along the solar path, t_d is the diffuse transmittance, and the subscripts s and v refer to the solar and view directions. For a homogeneous surface this equation simplifies to

$$\rho = \rho_{atm} + \frac{T(\mu_s)}{1 - \rho_T s}\rho_T T(\mu_v) \quad \textbf{(7)}$$

From these two equations it can be seen that the error in reflectance due to ignoring the environment effect can be written as

$$\Delta\rho = \frac{T(\mu_s)}{1 - <\rho> s}(<\rho> - \rho_T) t_d(\mu_v) \quad \textbf{(8)}$$

In order to determine the effects of the environmental effect, we first determine the reflectance and extent of the target and surround. This is done using SPOT HRV images of both sites. The surround reflectance was determined from histograms of the data for square boxes surrounding

each target. The sizes of the boxes were l, 4, 25, and 100 km^2. The results are shown for both White Sands and La Crau in Figures 4 and 5 respectively. From the figures it can be seen that the surround is brighter for White Sands and darker for La Crau.

Similar approaches were used for all three XS bands for SPOT HRV and the reflectance as a function of distance from the target was parameterized using

$$\rho(r) = \rho_T(1 + ar) \quad \textbf{(9)}$$

where $\rho(r)$ is the reflectance at a distance r from the target, ρ_T is the reflectance of the target as measured at the time of satellite overpass, and a is a fit parameter determined from the histogram data. This formulation is used here because it allows for an analytical solution of the formulas used within the 5S radiative transfer code to determine the adjacency effect. Assuming that $<\rho>$ varies more slowly than the surface reflectance we can use (6) to get

$$\rho^{*}_{TOA}(r) - \rho^{*}_{TOA}(r=0) = T(\mu_s)(\rho_G(r) - \rho_G(r=0))e^{-\delta/\mu_v} \quad \textbf{(10)}$$

Combining this with (9) we have

$$\rho_G(r) = \rho_G(0) + \frac{a}{T(\mu_s)e^{-\delta/\mu_v}} r \quad \textbf{(11)}$$

where $\rho_G(0)$ corresponds to the measurements on the test site, a is determined from the image data and atmospheric parameters are determined from ground-based measurements at the test site.

Strictly speaking, we need to determine the fit parameter in (9) and (11) we need the reflectance at the surface. Unfortunately, the histogram data that are available are for the top of the atmosphere and thus contain atmospheric effects. In this work we examine two methods for converting the at-sensor DNs to values at the surface. The first method assumes that the DNs at point i in the image can be written as the sum of an atmospheric and surface components:

$$DN_i^{*} = DN^{atm} + T_g \times T_a \times DN_i^{ground} \quad \textbf{(12)}$$

Where DN_i* is the digital number at the top of atmosphere for the pixel i, DN^{atm} is the digital number due solely to the atmosphere, Ta is the global transmittance defined to be $T_{a'}=T(\mu_s)T(\mu_v)$, Tg is the gaseous transmittance and DN_i^{ground} is the digital number due to the energy reflected by the surface. Differencing two pixels in an image gives

$$\Delta DN^{*} = T_g \times T_a \times \Delta DN^{ground} \quad \textbf{(13)}$$

Another way to consider the problem is to assume that all of the direct bean energy comes from the target area and that due to the diffuse field must come from the background region. In this case we have

$$DN_i^{*} = DN^{atm} + T_g \times T(\mu_s) \times \left(DN_i^{ground} \times e^{-\delta/\mu_v} + <DN> t_d(\mu_v) \right) \quad \textbf{(14)}$$

and the difference between two pixels becomes

$$\Delta DN^{*} = T_g \times T(\mu_s) \times e^{-\delta/\mu_v} \times \Delta DN^{ground} \quad \textbf{(15)}$$

The 6S code in its original form allowed for adjacency effects to be included. However, the original version assumes

$$\rho(r) = \rho_T F(r) + \rho_{env}(1 - F(r)) \quad \textbf{(16)}$$

Thus, we have modified the code to use the formulation for $\rho(r)$ given in the last section.

Tables 2 shows the results of excluding the environment effect in determining the apparent reflectance for La Crau and White Sands respectively. The results are shown for two typical visibilities for each site, a low and high visibility that correspond to 50 km and 100 km for White Sands and 23 km and 50 km for La Crau. Typical view and solar geometries for HRV are also used. The results are different for the two sites because the environment is brighter around White Sands and darker around La Crau. The results seem to show a bigger effect for White Sands, but the visibilities are most of the time around 100 km for White Sands and 23 km for La Crau. In the case of White Sands, the calibration coefficient determined from assuming the surface to be homogeneous is smaller than that determined while accounting for spatially varying surface reflectance. The effect is also larger for XS1 than for the other bands. Both of these results make sense in that band 1 has higher atmospheric scattering, thus increasing the effect of the environment. Also, the environment around White Sands will increase the radiance at the sensor, thus a reflectance-based approach that ignores adjacency effects underestimates the radiance relative to the reported digital numbers. In this case, the calibration coefficients (digital number/radiance) will be underestimated at White Sands when the spatial variability is ignored. In all cases, this effect was modeled to be less than 4%, and in most cases less than 3%. The mean effect was a correction of 2.4% for XS1 and 1.4 % for XS3 at White Sands.

Similar conclusions can be drawn for La Crau, except rather than underestimating the calibration coefficient, it will be overestimated. In the case of La Crau, though, it is XS2 which shows the largest effect. This is due to the spectral reflectance of the sight relative to the surround being different for this band than the others. For La Crau, the effect of ignoring the surround has less than a 6% effect and in most cases is less than 3%. The mean effect was a correction of 2.4% for XS1 and 2.1% for XS3.

The main uncertainty with these results is that we studied only one HRV image for each site to model the environment effect. Both sites have temporally varying surface reflectance with White Sands changing due to surface and sub-surface moisture and La Crau changing with growing season due to the surrounding vegetation. This effect should be larger for La Crau so an additional image was studied in a similar fashion as described above. From Figure 6, we see that for a distance less than 5 km the slope tends to be positive in the XS3 band in summer, while it is negative in winter. Table 3 shows that while the slope in the XS1 band is always negative, this is not the case for XS3 where the slope is negative, nearly zero, or positive. Thus, if the vegetation is dense, the environment becomes brighter than the site and the correction needed for adjacency effects changes in sign. The uncertainty in the at-sensor reflectance for the winter case was used to derive the results shown in Table 3, and the difference between the results of the two days has a mean of 1.6%. This difference is as large as 2.5% for some days. The most important result is the fact that for the XS3 band the difference between the two extreme days is very important because of the high reflectance of vegetation at 850 nm.

Ground reflectance

Previous work with the uncertainties at White Sands determined the uncertainty in the reflectance measurements to be 2.1% [Biggar et al, 1994]. This uncertainty was primarily due to a 2.0% uncertainty in the reference panel calibrations and 0.5% uncertainty in both the instrumentation and the lack of a diffuse-light correction. Because of the large oversampling of the test site, this past work, did not consider uncertainty due to sampling. For this work we include a nominal uncertainty due to sampling the test site and use a 2.5% uncertainty in the retrieved reflectance of the test site.

For La Crau, Gu (1991) determined that the number of measurements, N, that are needed to estimate the average reflectance of a given area to precision p for a 95Vo confidence interval, can be found using (Dagnelie 1970).

$$N = 2 \times \left(\frac{1.96\sigma}{pR} \right)^2 \quad \textbf{(17)}$$

Where σ is the standard deviation of the statistical distribution and has values of 10.7 for XS1, 10.0 for XS2, and 5.1 for XS3. These values are then used to determine the uncertainty in reflectance based on the number of measurements made for each campaign. The value for the uncertainty used for other factors such as radiometric uncertainty, reference panel calibration, etc. is 1.6%.

The reflectance measurement uncertainties can be combined with the BRDF and environment effects to produce a global uncertainty due to surface reflectance. To do this, we use two quadratic sums, one without the BRDF and environment effects and the other with these effects. Figures 7, 8, and 9 show the uncertainty in the predicted at-sensor radiance for the XS-1 band of SPOT-2 HRV due to uncertainties in the reflectance. These figures are for the entire lifetime of SPOT-2 HRV for both White Sands and La Crau. Figure 7 also includes the uncertainty due to the reflectance measurements only, Figure 8 includes the uncertainty due to the environment effect, and Figure 9 that due to the BRDF. For all cases, the global error does not exceed 5.5%.

The figures also show that the measurements errors for La Crau are comparable with those at White Sands (between 2 and 3%), the environment effect is between 1 and 4% (with a mean of 2.5 %), and the BRDF effect ranges from 0 and 4%.

SYNTHESIS OF RESULTS

Figure 10 shows the component uncertainties in terms of percent of the total error for bands XS1 and XS3 for data collected at White Sands and La Crau on two representative days In this figure, uncertainties less than 0.1% should be considered equivalent to zero. The bands XS1 and XS3 are shown because they are affected by ozone and water vapor absorption. What we can see in this figure is the fact that the most important parameter is the ground reflectance, particularly for White Sands. This makes sense because the 1196-m altitude of the site and its high reflectance decreases the impact of the atmosphere. In addition, the imaginary part of the refractive index and the spectral response functions of the filters are important effects.

SPOT CALIBRATION FACTORS

To calculate new calibration factors, we use both the 6S and the successive orders of scattering codes. 6S is used to calculate the gaseous transmission, taking account of the ozone amount and the water vapor continuum and the successive orders code used to compute scattering effects. In addition, we determine uncertainties for each calibration coefficient based on the above results. Figures lla and 12a show the new calibration coefficients for the XS1 and XS3 bands of SPOT-2 along with their error bars for the case where there has not been an adjacency effect or BRDF effect correction. Also shown in the figure is the best fit to the onboard lamp calibration data. Figures l1b and 12b are similar but show the results for the new calibration factors corrected for the BRDF and the environment effects for the XS1 and XS3 bands for SPOT-3. The error bars in this case are the same as for the other case because the uncertainty due to BRDF and environment effects cause a bias in the results and are not randomly distributed. For both sets of curves, with and without BRDF and adjacency effect correction, there is no significant difference in the dispersion of the points, but simply a 2-3% shift in the placement of the data.

These results are also tabulated in Tables 4, 5, and 6. Tables 7 shows the differences between the best fit lamp data and the two sets of vicarious results, corrected and uncorrected. The results are given for both SPOT-2 and SPOT-3 and the XS I and XS3 bands. Again, Tables 7 and 8 show no clear indication that the BRDF and adjacency correction reduce the dispersion from the best-fit lamp curve. As discussed earlier, this is most likely due to the fact that these two effects cause systematic biases in the vicarious calibration rather than a random error. From the results, we see that the error budget is less favorable for La Crau than for White Sands for the bands XS1 and XS2. However, this difference is not significant. Also, several of the points derived from data at La Crau differ greatly from the lamp curve (e.g., data from 28/01/92 and 21/07/95 for SPOT-2, and 24/06/94 and 7/07/95 for SPOT-3). One explanation for these points is that we did not include absorption effects in the determination of the calibration coefficient.

CONCLUSIONS

The primary result of this work is a reprocessing of all of the calibration data for the SPOT HRV cameras using the same assumptions about aerosols and gaseous absorption, and using the same radiative transfer code to predict the radiance at the sensor. We also removed potential biases introduced in the calibration procedure by the non-lambertian nature of the surface and that due to surface inhomogeneities. All of the results are combined with other techniques (Dinguirard et al., this issue) to derive the HRV calibration coefficients.

As a conclusion, we can say that the error on the calibration factor at White Sands appears to depend primarily on three parameters: ground-reflectance, imaginary part of the refractive index, and spectral response. For La Crau, this work shows that more parameters are important and this is mostly due to the fact that the site is near sea level. This low altitude increases the amount of aerosols and thus increases the importance of the aerosol parameterization. This is especially true for the single scattering albedo.

The error budget over White Sands shows that we have differences from the lamp curves of less than 3.5% and most of the time this value is less than 2.7%. These values exclude corrections due to BRDF and environment effects. When these two effects are included, the differences are between 3.0% and 6.5% for XS1 and XS2. For

XS3, the differences are smaller, in the range from 2.5% and 4.5%. The conclusion for La Crau is quite the same, when we consider the global error, even if the error made on the calibration factor seems to be higher for that site. For the case with no correction, the differences are between 3.0% and 9.5% for XS1 and XS2, and 2.5% and 8.0% for XS3. When the correction is included, the differences are between 2.8% and 8.0% for the first two bands and between 2.5% and 6.0% for XS3.

ACKNOWLEDGEMENTS

We would like to acknowledge the help of C. Devaux and J.L. Deuzé of the LOA for their assistance with this work. We would also like to acknowledge the work of G. Guyot and M. Verbrugghe for their help with the data at La Crau.

References

S.F. Biggar, P.N. Slater, D.J. Gellman, *Uncertainties in the in-flight calibration of sensors with reference to measured ground sites in the 0.4 to 1.1 μm region.* Vol. 48, pp. 242-252.Remote Sensing of Environment 1994.

M. Chami, *Caractérisation du site d'étalonnage de White Sands (Nouveau Mexique).* Stage de DEA, université de Paris VII, Juin 1994.

Dagnelie P., *Théorie et méthodes statistiques vol2. Les presses Agronomiques de Gembloux,* A.S.B.S.L., Ed. J. Duclot, S.A, Gembloux :451p. 1970.

J.L. Deuzé, M.Herman, R. Santer, *Fourier series expansion of the transfer equation in the atmosphere-ocean system* J. QUANT. Spectrosc. Transfert 41 : 483-494, 1989.

J.L. Deuzé, C. Devaux, R. Santer, X.F. Gu, G. Guyot, J.F. Hanocq, M. Verbrugghe, *Campagne d'étalonnage SPOT-2 Janvier 1992*.

C. Devaux, A. Vermeulen, J.L. Deuzé, M. Herman, *Retrieval of the single scattering albedo of atmospheric aerosols from ground-based measurements. Analysis of observational data.* Journal of Geophysical Research Accepted for publication 1996.

D. I. Gellman, S. F. Biggar, and P. N. Slater, *Calibrated intercepts for solar radiometers used in remote sensor calibration* Proc. SPIE, Vol. 1493-19, Orlando, Florida 1991.

X. Gu, *Etalonnage et intercomparaison des données satellitaires et utilisant le site test de La Crau* Thèse de doctorat de l'Université Paris VII 17 juin 1991.

Q.J. Hart, *Surface and aerosol models for use in radiative transfer code* M.S. thesis, University of Arizona, 66pp 1990.

P. Henry, M. Dinguirard, A. Meygret, *Synthèse sur l'étalonnage absolu des données SPOT* RAPPORT CNES CT/IA/QTIS/PO n°136 9 février 1995

B.M. Herman, S.R. Browning, *A numerical solution to the equation of radiative transfer* J. Atmos. Sci. 22:559-566 1965

R. Santer, *Caractérisation des aérosols à partir de la polarisation du rayonnement solaire diffusé. Application aux atmosphères de la Terre, de Vénus et de Saturne*. Thèse de doctorat de l'université des sciences et techniques de Lille 13 juillet 1984

R. Santer and P. Lecomte, *Reflectances and degrees of polarization during the La Crau campaign 1991* Septembre 1992

R. Santer, X. Gu, J.L. Deuzé, C. Devaux, E. Vermote, et al., *SPOT calibration at the La Crau test site (FRANCE)* Remote Sensing of Environment 41:227-237. 1992

R. Santer, M. Chami, D. Dessailly, *Etudes sur les sites désertiques. Multidirectionnalité des reflectances et de la polarisation de trois types de surfaces à White Sands* Rapport final annexe III Contrat CNES n'833/CNES/94/1227/00. Décembre 1995

P.N. Slater, G. Begni, M.C. Dinguirard, R.D. Jackson, *Absolute calibration of the SPOT-1 HRV cameras* vol. 660 Earth Remote Sensing Using the Landsat Thematic Mapper and SPOT-sensor Systems, 1986

P. N. Slater, S.F. Biggar, R.G. Holm, R.D. Jackson, Y. Mao, M.S. Moran, J.M. Palmer, B. Yuan, *Reflectance- and radiance- based methods for the in-flight absolute calibration of multispectral sensors* Remote Sensing of Environment 22:11-37, 1987

D. Tanré, C. Deroo, P. Duhaut, M. Herman, J J. Morcrette, P.Y. Deschamps, *Simulation of the Satellite Signal in the Solar Spectrum (5S)* Laboratoire d'Optique Atmosphérique, 59655 Villeneuve d'Ascq Cédex, France 1987.

K.J. Thome, M.W. Smith, J.M. Palmer, and J.A. Reagan, *Method and instrument for retrieving total columnar water vapor from solar transmittance*, SPIE proceedings Vol. 1968-56, Orlando Florida, April 1993

E. Vermote, *Effets d'atmosphère en télédétection* Thèse de doctorat de l'Université des sciences et techniques de Lille 20 Juin 1990

E. Vermote, et al., *Second Simulation of the Satellite Signal in the Solar Spectrum* 6S User guide Version 1 November 3, 1995

C. H. Whitlock, S.R. Lecroy and J. Wheeler, *Narrowband angular reflectance properties of the alkali flats at White Sands, NEW MEXICO* Remote Sensing of Environment, vol. 50, pp 171-181, 1994

Location	Month (column amount)	SPOT-2		SPOT-3	
		XS1	XS2	XS1	XS2
White Sands	February (0.340)	0.617	0.71		
	April (0.340)	0.50	0.59	0.57	0.52
	May (0.320)	0.46	0.54		
	June (0.310)	0.44	0.52		
	August (0.280)	0.43	0.51		
	October (0.260)			0.45	0.42
	November (0;280)	0.43	0,51	0.56	0.52
La Crau	January (0.350)	0.74	0.90		
	June (0.330)	0.47	0.57		
	July (0.310)	0.45	0.54	0.50	0.44

Table I. Uncertainties for the XSl and XS2 bands for the two sites due to uncertainties in columnar ozone amounts.

Solar Zenith Angle	Satellite view Angle	Relative Azimuth	Visibility	White Sands		La Crau	
				XSl	XS3	XS1	XS3
30	0	40	low	-4.61	-2.25	2.37	1.83
			high	-3.13	-1.42	1.52	1.09
	30	40	low	-4.95	-2.45	2.54	2.02
			high	-3.40	-1.54	1.65	1.20
	30	140	low	-4.88	-2.41	2.51	2.00
			high	-3.31	-1.51	1.64	1.19
60	0	40	low	-4.13	-2.15	1.91	1.75
			high	-2.82	-1.35	1.27	1.04
	30	40	low	-4.40	-2.35	2.03	1.95
			high	-2.99	-1.48	1.36	1.17
	30	140	low	-4.42	-2.32	1.92	1.86
			high	-3.05	-1.46	1.33	1.13

Table II. Adjacency effect uncertainties for the XS1 and XS3 bands for the two sites for typical view conditions, solar angles, and aerosol loadings. The low and high visibility cases for White Sands correspond to 50 and 100 km. Those for La Crau are 23 and 50km. Ground reflectances are for White Sands 0.6±0.02 for XSl and 0.68±0.02 for XS3, 0.15B).02 and 0.3±0.02 for La Crau.

Day	XS1 slope	XS3 slope
28/01/92	-0.0201	-0.014
23/06/91	-0.0277	-0.0064
25/06/91	-0.0285	0.0010
09/07/96	-0.0339	0.0055

Table III. Slope of spatial variability of La Crau site for multiple dates.

SPOT1	XS1	error	XS2	error	XS3	Error	Pan	error
*08/03/86	0,527	3,5	0,436	3,3	0,601	2,8	0,564	3,3
*15/03/86	0,531	3,3	0,446	3,1	0,619	2,8	0,601	3,1
*20/03/86	0,528	3,6	0,416	3,3	0,592	3,0	0,616	3,2
*17/07/87	0,51 2	3,8	0,370	3,6	0,583	3,1	0,623	3,8
+10/02/88	0,462	3,8	0,343	3,7	0,535	3,3	0,575	3,6
*16/11/88	0,467	2,7	0,341	2,7	0,542	2,7	0,579	2,6
*21/11/88	0,462	3,0	0,337	2,9	0,534	2,8	0,574	2,8
22/03/89	0,527	3,2	0,380	3,4	0,567	2,7		
07/06/89	0,487	3,9	0,379	4,3	0,573	3,0		
13/06/89	0,476	6,7	0,387	7,8	0,606	4,9		
*06/02/90	0,475	3,0	0,349	2,9	0,548	2,7	0,566	2,8
*07/02/90	0,475	3,1	0,350	3,0	0,554	2,8	0,586	2,8
*21/06/90	0,438	5,0	0,320	4,7	0,495	3,7	0,543	4,8
*22/06/90	0,426	6,4	0,310	5,8	0,477	4,4	0,528	6,0
*15/06/92	0,406	5,3	0,293	7,0	0,464	4,1		
*16/08/92	0,41 3	7,3	0,308	6,1	0,468	4,6	0,521	4,8
08/07/97	0,392	2,6	0,287	3,2	0,477	2,4	0,505	3
09/07/97	0,384	4,8	0,285	5,4	0,483	3,0	0,509	2,7

Table IV a. SPOT1 calibration coefficients not corrected of BRDF and Adjacency effect with uncertainty estimation for La Crau and *White Sands.

SPOT1	XS1	error	XS2	error	XS3	Error	Pan	Error
*08/03/86	0,517	2,8	0,430	2,7	0,595	2,7	0,555	2,7
*15/03/86	0,530	2,6	0,445	2,6	0,617	2,6	0,599	2,6
*20/03/86	0,526	2,7	0,414	2,8	0,588	2,7	0,614	2,7
*17/07/87	0,515	2,7	0,369	2,7	0,580	2,7	0,623	2,7
*10/02/88	0,453	2,9	0,337	2,9	0,524	2,9	0,563	2,9
*16/11/88	0,462	2,6	0,339	2,6	0,541	2,6	0,575	2,6
21/11/88	0,454	2,7	0,334	2,8	0,531	2,8	0,567	2,6
22/03/89	0,534	3,1	0,385	3,2	0,568	2,7		
07/06/89	0,492	3,7	0,387	3,9	0,576	2,9		
13/06/89	0,502	5,5	0,419	5,0	0,624	4,1		
*06/02/90	0,466	2,6	0,345	2,7	0,544	2,6	0,562	2,6
*07/02/90	0,468	2,6	0,346	2,7	0,550	2,7	0,581	2,6
*21/06/90	0,430	3,1	0,316	3,0	0,490	2,9	0,536	3,0
*22/06/90	0,423	3,5	0,307	3,3	0,473	3,1	0,524	3,4
*15/06/92	0,427	3,7	0,319	3,4	0,481	2,9		
*16/08/92	0,402	3,5	0,301	3,3	0,460	3,2	0,525	3,4
08/07/97	0,397	2,4	0,295	2,6	0,480	2,3	0,517	2,5
09/07/97	0,405	2,7	0,304	2,8	0,495	2,5	0,538	2,7

Table IV b. SPOT1 calibration coefficients corrected of BRDF and Adjacency effect with uncertainty estimation for La Crau and *White Sands.

SPOT2	XS1	error	XS2	error	XS3	Error	Pan	error
*09/02/90	0,466	4,3	0,378	3,8	0,857	3,3	0,411	3,6
*19/02/90	0,527	2,9	0,420	2,9	0,723	2,7	0,478	2,8
*20/02/90	0,535	2,9	0,426	3,0	0,752	2,7	0,478	2,8
*23/06/90	0,500	5,3	0,396	4,8	0,684	3,8	0,454	5,0
*24/06/90	0,496	5,1	0,396	4,4	0,691	3,4	0,451	4,6
*7/05/91	0,486	4,5	0,384	4,0	0,692	3,1	0,443	4,2
*08/05/91	0,492	5,2	0,387	4,3	0,680	3,3	0,449	4,6
23/06/91	0,459	4,5	0,339	5,0	0,633	3,3	0,426	4,2
25/06/91	0,469	3,9	0,374	3,9	0,674	2,6	0,454	3,4
*05/11/91	0,495	3,3	0,393	3,2	0,704	2,9	0,457	3,2
28/01/92	0,419	8,4	0,337	9,5	0,597	7,8	0,434	4,6
17/06/92	0,467	6,2	0,364	7,9	0,690	4,5	0,430	6,6
27/06/92	0,451	7,9	0,314	9,0	0,668	5,5	0,412	7,8
*17/08/92	0,483	3,0	0,375	2,8	0,677	2,7	0,443	2,9
*18/08/92	0,468	5,6	0,366	4,9	0,659	3,9	0,430	5,1
*03/04/93	0,434	5,1	0,387	4,5	0,695	3,5	0,427	4,7
27/06/93	0,448	4,3	0,354	4,4	0,659	2,8	0,430	4,0
20/06/94	0,459	3,8	0,357	4,3	0,651	2,8	0,442	3,6
21/06/94	0,447	5,5	0,352	6,5	0,670	3,6	0,435	5,7
30/06/94	0,436	5,0	0,352	5,8	0,679	3,7	0,430	5,6
*01/04/95	0,407	4,5	0,375	4,0	0,701	3,2	0,415	4,2
15/07/95	0,433	4,2	0,339	4,6	0,658	2,9	0,415	4,0
21/07/95	0,474	6,5	0,372	7,9	0,712	5,0	0,462	6,8
*10/10/95	0,472	5,1	0,372	4,4	0,678	3,6	0,430	4,3
28/06/96	0,438	4,3	0,350	5,5	0,692	3,4	0,434	4,6
09/07/96	0,458	4,2	0,368	4,0	0,707	2,5	0,456	3,4
06/07/96	0,435	2,9	0,348	3,3	0,692	2,5	0,424	2,7
07/07/97	0,452	2,9	0,364	3,7	0,721	2,8	0,449	3,3
08/07/97	0,423	4,4	0,343	4,2	0,657	2,6	0,422	3,9

Table V a. SPOT2 calibration coefficients not corrected of BRDF and Adjacency effect with uncertainty estimation for La Crau and *White Sands

SPOT2	XS1	error	XS2	error	XS3	Error	Pan	Error
*09/02/90	0,450	2,9	0,369	2,9	0,857	3,3	0,402	2,9
*19/02/90	0,519	2,6	0,417	2,7	0,719	2,6	0,474	2,6
*20/02/90	0,532	2,6	0,422	2,7	0,750	2,6	0,475	2,6
*23/06/90	0,480	3,2	0,383	3,1	0,668	2,9	0,439	3,1
*24/06/90	0,496	2,9	0,395	2,8	0,688	2,7	0,450	2,8
07/05/91	0,484	2,8	0,382	2,8	0,689	2,7	0,441	2,7
*08/05/91	0,493	2,9	0,385	2,8	0,676	2,7	0,448	2,8
23/06/91	0,467	3,4	0,352	3,1	0,639	2,6	0,442	2,5
25/06/91	0,486	2,8	0,388	2,8	0,682	2,5	0,470	2,2
*05/11/91	0,484	2,7	0,387	2,7	0,697	2,7	0,449	2,7
28/01/92	0,417	7,6	0,338	7,3	0,588	5,8	0,458	2,7
17/06/92	0,492	4,7	0,398	4,1	0,718	3,1	0,463	3,5
27/06/92	0,483	6,1	0,346	5,4	0,700	4,2	0,449	4,7
*17/08/92	0,486	2,5	0,376	2,6	0,678	2,6	0,444	2,5
*18/08/92	0,466	3,3	0,362	3,2	0,652	3,0	0,426	3,2
*03/04/93	0,429	3,1	0,382	3,0	0,689	2,8	0,422	3,0
27/06/93	0,467	2,9	0,371	2,8	0,671	2,5	0,449	2,4
20/06/94	0,472	3,1	0,372	2,9	0,661	2,5	0,459	2,2
21/06/94	0,474	3,5	0,381	3,1	0,692	2,6	0,467	2,4
30/06/94	0,452	4,2	0,373	3,8	0,693	3,1	0,459	2,9
*01/04/95	0,403	2,9	0,372	2,8	0,696	2,7	0,411	2,8
15/07/95	0,450	3,1	0,356	3,0	0,669	2,6	0,434	2,4
21/07/95	0,492	5,1	0,401	4,4	0,727	3,6	0,490	4,3
*10/10/95	0,467	3,1	0,367	3,0	0,671	2,9	0,428	3,0
28/06/96	0,450	3,5	0,372	5,5	0,708	3,0	0,458	2,4
09/07/96	0,477	2,8	0,382	4,0	0,716	2,4	0,472	2,2
06/07/97	0,439	2,5	0,355	2,8	0,694	2,4	0,431	2,3
07/07/97	0,460	2,6	0,376	2,8	0,729	2,7	0,463	2,5
08/07/97	0,442	2,5	0,359	2,7	0,668	2,4	0,440	2,4

Table V b. SPOT2 calibration coefficients corrected of BRDF and Adjacency effect with uncertainty estimation for La Crau and *White Sands

SPOT3	XS1	error	XS2	error	XS3	Error	Pan	error
*21/10/93	0,889	3,3	1,161	3,2	0,971	2,9	0,624	3,2
’20/11/93	0,857	3,3	1,12	3,1	0,943	2,8	0,604	3,1
*21/11/93	0,811	3,6	1,057	3,3	0,894	3,0	0,569	3,2
23/06/94	0,76	4,7	0,971	5,5	0,882	3,4	0,562	4,7
24/06/94	0,742	5,7	0,941	6,4	0,770	3,7	0,546	4,6
*09/10/94	0,791	3	1,041	2,9	0,908	2,7	0,587	2,9
03/04/95	0,737	3,9	0,966	3,4	0,869	2,8	0,539	3,6
07/07/95	0,628	6,9	0,795	8,8	0,787	4,7	0,479	7,2
26/06/96	0,682	5,5	0,937	6,2	0,900	3,6	0,528	5,4
06/07/96	0,782	4	0,989	3,8	0,878	2,8	0,583	3,4
11/07/96	0,726	4,6	0,935	4,3	0,837	2,8	0,542	3,7

Table VI a. SPOT3 calibration coefficients not corrected of BRDF and Adjacency effect with uncertainty for La Crau and *White Sands.

SPOT3	XS1	error	XS2	error	XS3	Error	Pan	error
*21/10/93	0,878	2,7	1,149	2,7	0,963	2,7	0,617	2,7
*20/11/93	0,835	2,7	1,101	2,7	0,933	2,7	0,592	2,7
*21/11/93	0,787	2,7	1,035	2,7	0,882	2,7	0,558	2,7
23/06/94	0,790	3,8	1,031	3,4	0,901	3,4	0,590	2,7
24/06/94	0,785	4,0	1,012	3,6	0,794	3,0	0,575	2,7
*09/10/94	0,785	2,6	1,037	2,6	0,905	2,6	0,584	2,6
*03/04/95	0,724	2,8	0,955	2,7	0,863	2,6	0,532	2,7
07/07/95	0,673	4,7	0,881	3,9	0,823	3,2	0,523	3,0
26/06/96	0,724	3,4	1,009	3,0	0,928	2,8	0,564	2,5
06/07/96	0,813	2,8	1,026	2,8	0,889	2,6	0,603	2,3
11/07/96	0,761	3,1	0,977	3,0	0,850	2,6	0,564	2,3

Table VI b. SPOT3 calibration coefficients corrected of BRDF and Adjacency effect with uncertainty for La Crau and *White Sands.

Dispersion/Best fit lamp	XS1-SPOT2	XS3-SPOT2	XS1-SPOT3	XS3-SPOT3
Global	6,5%	4,9%	6,4%	5,8%
Global corrected	7,8%	5,3%	5,5%	5,4%
La Crau	6,4%	5,1%	8,3%	6,4%
La Crau corrected	7,4%	5,7%	6,8%	5,9%
La Crau corrected of adjacency effect	7,5%	4,1%	9,2%	6,4%
La Crau corrected of BRDF effect	6,5%	5,6%	9,1%	6,4%
White Sands	6,5%	4,7%	4,0%	5,3%
White Sands corrected	8,3%	4,7%	3,4%	4,7%
White Sands corrected of adjacency effect	9,0%	4,6%	3,4%	4,5%
White Sands corrected of BRDF effect	6,9%	4,6%	3,2%	5,5%

Table VII. Dispersion of the calibration coefficient compared to the best-fit lamp

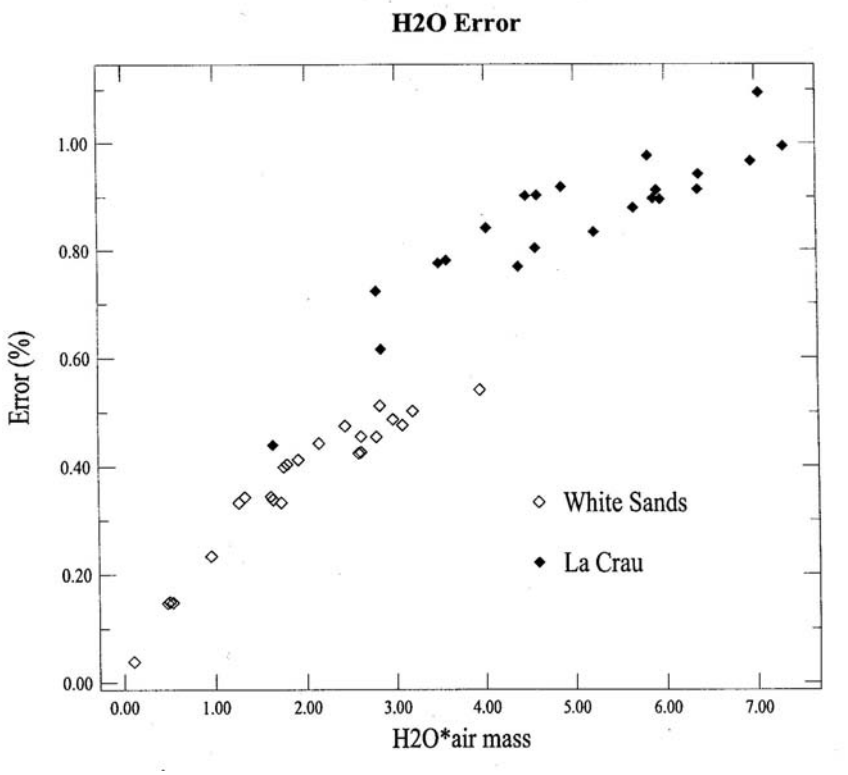

Fig I. Uncertainties for the XS3 bands for the two sites due to uncertainty in water vapor content.

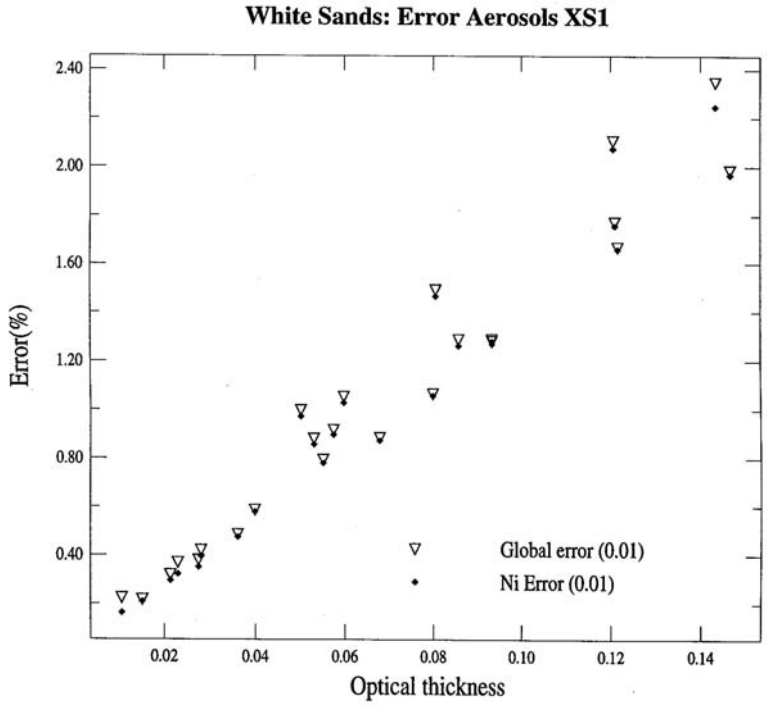

Figure II. Comparison of the aerosol uncertainty (optical thickness, Angstrom coefficient, refractive index, imaginary and real part) and the uncertainty due to the imaginary part of the refractive index for the XS1 band, for White Sands, with an error of ±0.01 on the optical thickness.

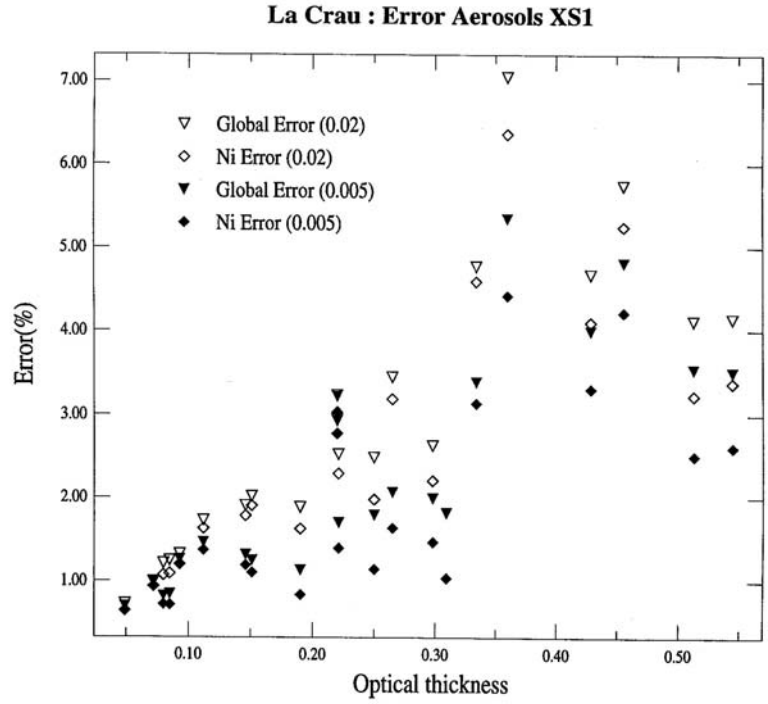

Figure III. Comparison of the aerosol -uncertainty (optical thickness, Angstrom coefficient, refractive index, imaginary and real part) and the uncertainty due to the imaginary part of the refractive index for the XS1 band; for La Crau, with an error of ±0.02 and ±0.005 on the optical thickness.

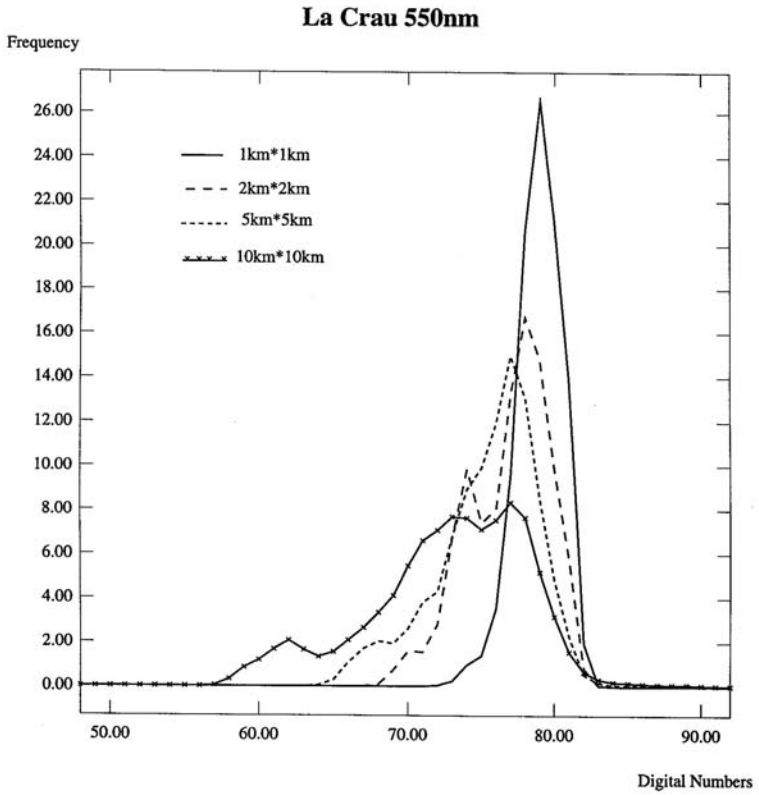

Figure IV. Spatial variability for White Sands (Histograms made on 4 different diametered-crown) at 550nm.

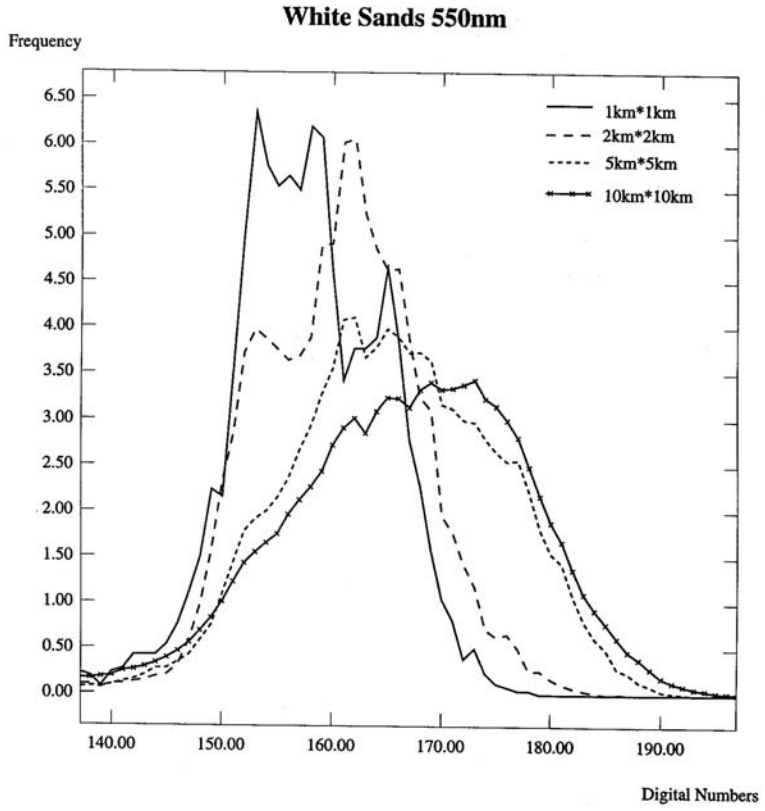

Figure V. Spatial variability for La Crau (Histograms made on 4 different diametered-crown) at 550nm.

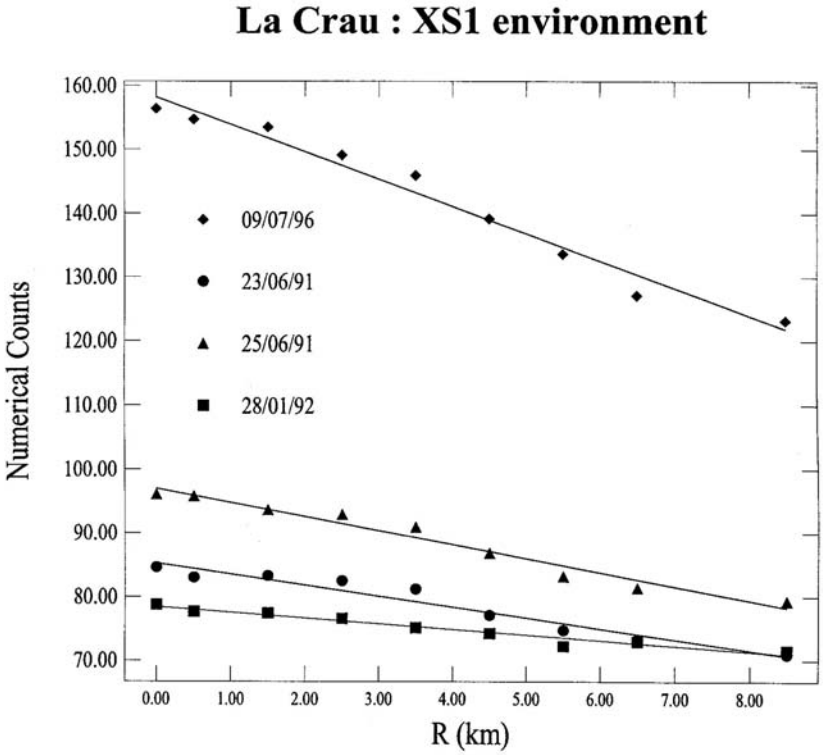

Figure VI a. XS1 Spatial variability of La Crau versus the distance from the site.

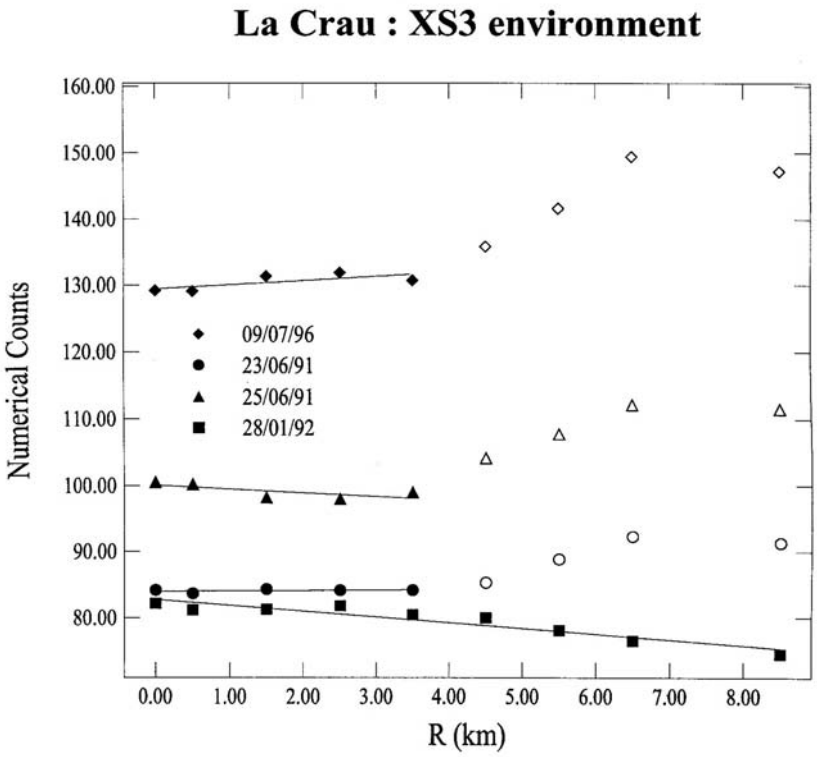

Figure VI b. XS3 Spatial variability of La Crau versus the distance from the site.

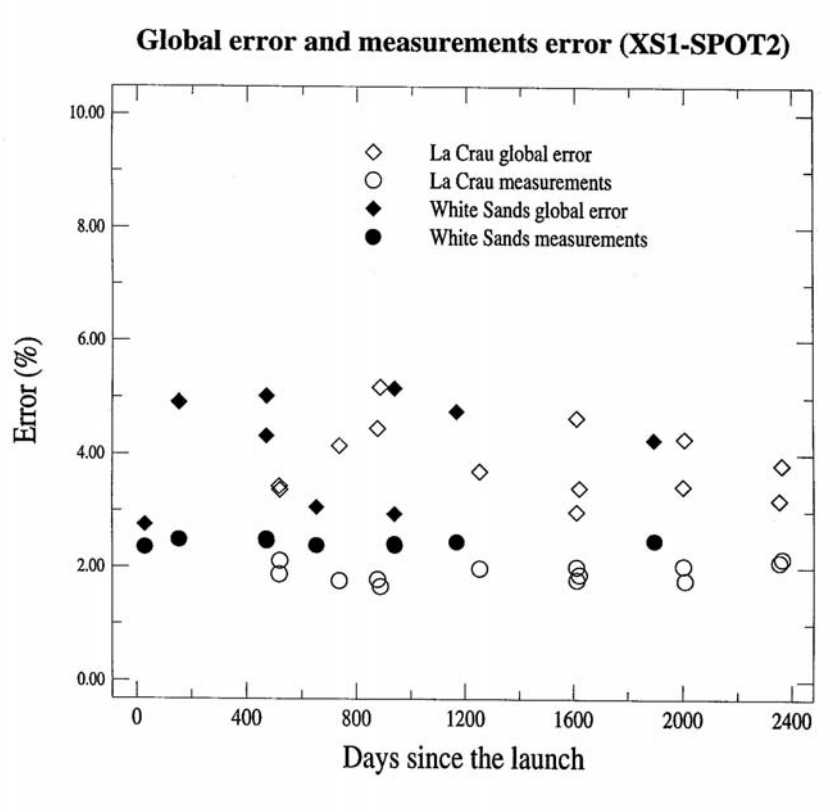

Figure VII. Comparison of the uncertainty on ground reflectance (BRDF, Adjacency, measurements) and measurements uncertainty.

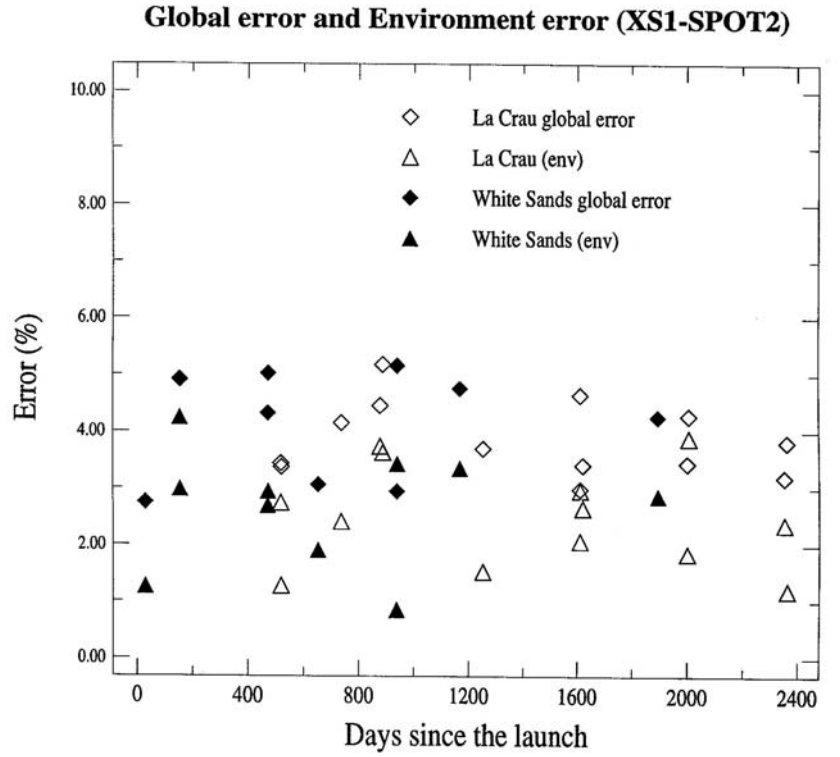

Figure VIII. Comparison of the uncertainty on ground reflectance (BRDF, Adjacency, measurements) and adjacency uncertainty.

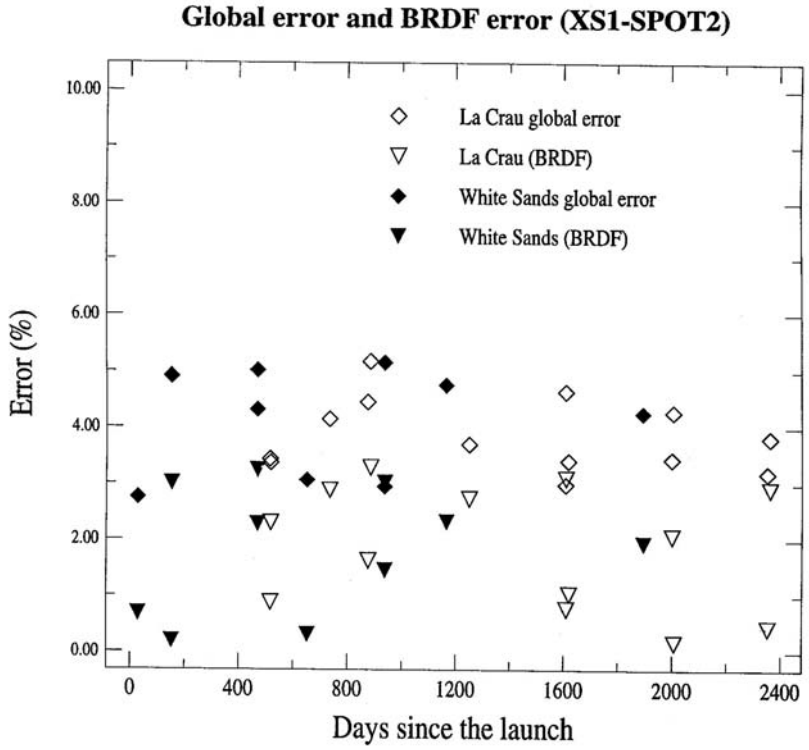

Figure IX. Comparison of the global uncertainty on ground reflectance (BRDF, Adjacency, measurements) and BRDF uncertainty.

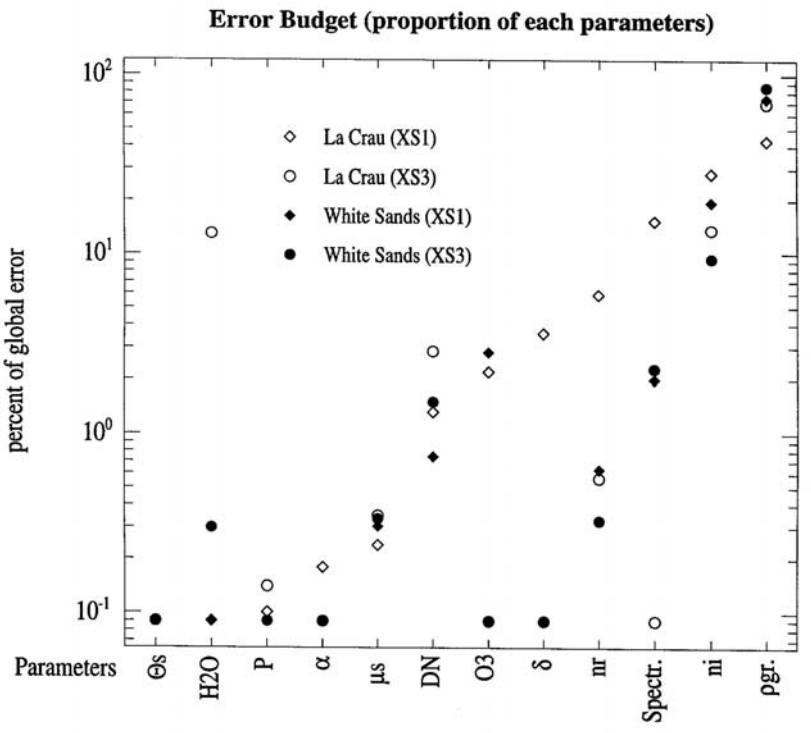

Figure X. Percentage of each parameters in the global error budget

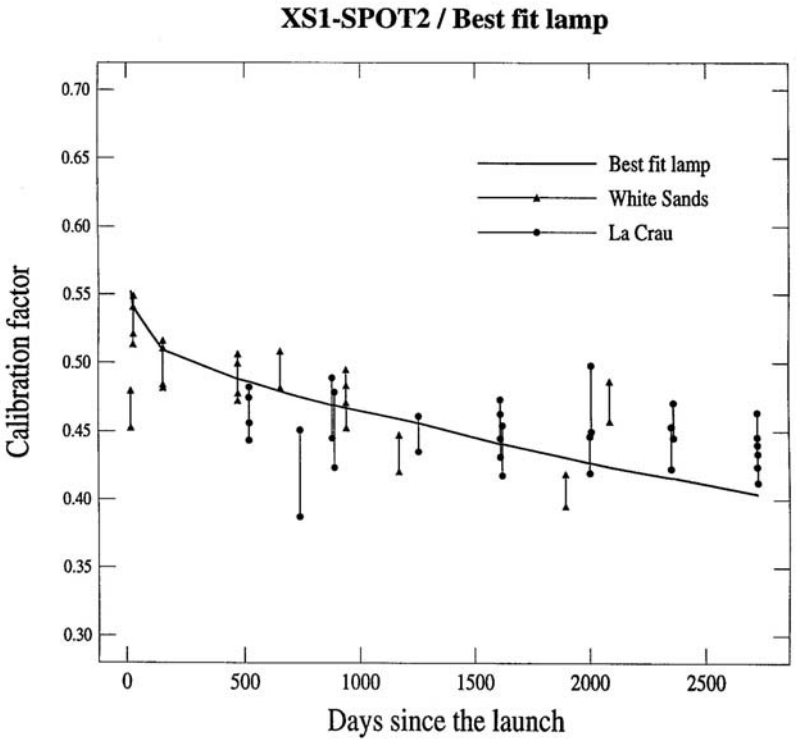

Figure XI a. XS1-SPOT2 calibration factors not corrected of BRDF and adjacency effect with the best-fit lamp curve

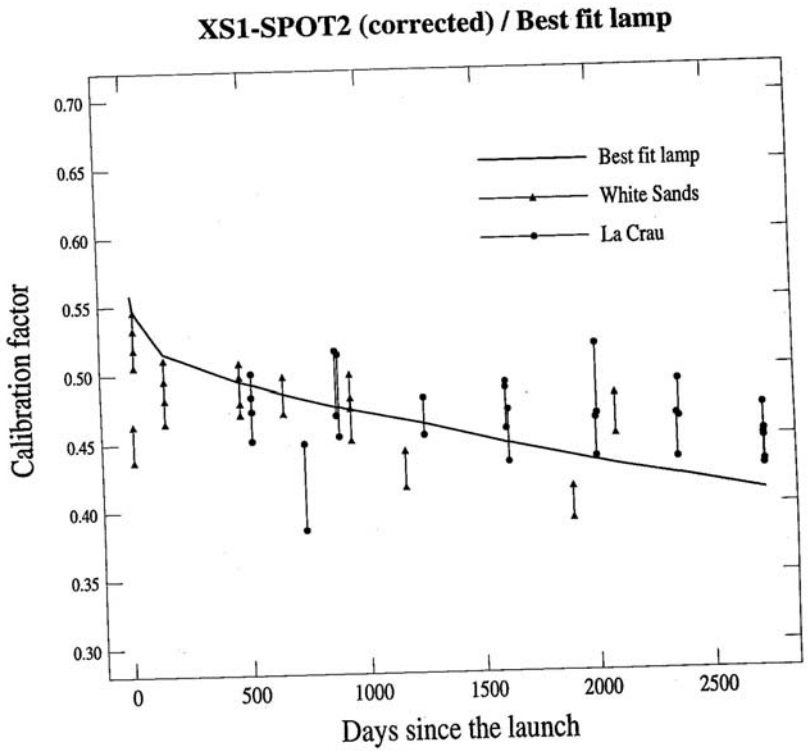

Figure XI b. XS1-SPOT2 calibration factors corrected of BRDF and adjacency effect with the best-fit lamp curve.

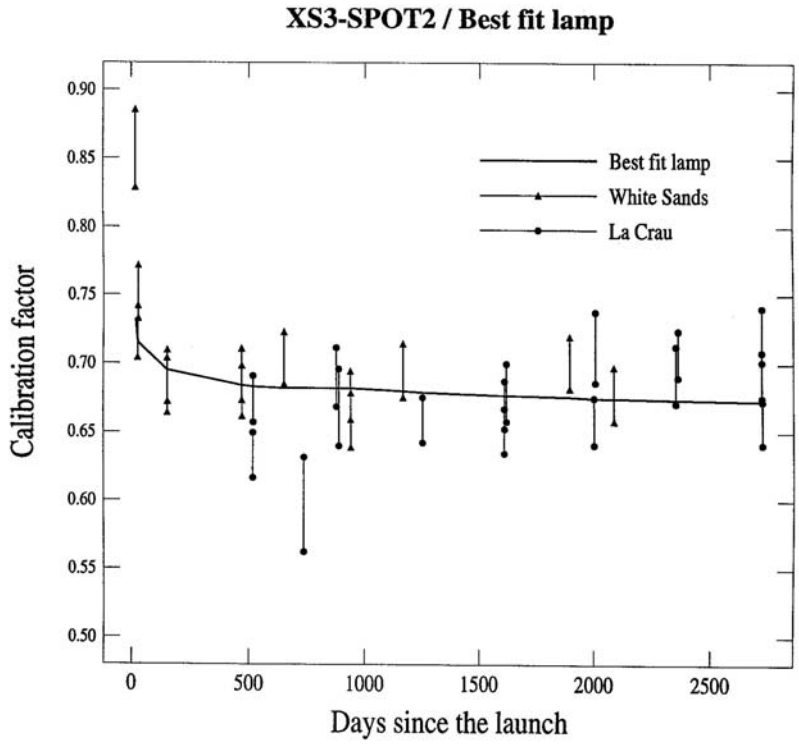

Figure XII a. XS3-SPOT2 calibration factors not corrected of BRDF and adjacency effect with the best-fit lamp curve.

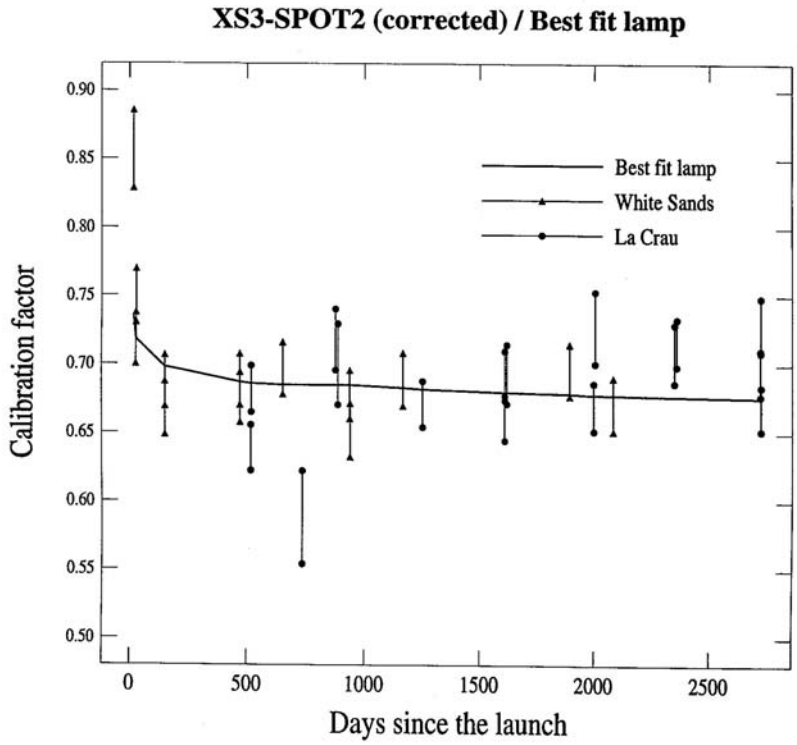

Figure XII b. XS3-SPOT2 calibration factors corrected of BRDF and adjacency effect with the best-fit lamp curve.